

Received: 2020.05.07
Accepted: 2020.09.21
Available online: 2020.09.30
Published: 2020.10.09

Morphological and Biochemical Properties of Human Astrocytes, Microglia, Glioma, and Glioblastoma Cells Using Fourier Transform Infrared Spectroscopy

Authors' Contribution:
Study Design A
Data Collection B
Statistical Analysis C
Data Interpretation D
Manuscript Preparation E
Literature Search F
Funds Collection G

BEF 1 **Dongsheng Kong***
CDF 2 **Wenyu Peng***
ABG 1 **Rui Zong***
BCD 3 **Gangqiang Cui**
AG 1 **Xinguang Yu**

1 Department of Neurosurgery, Chinese People's Liberation Army (PLA) General Hospital, Beijing, P.R. China
2 Science and Technology on High Power Microwave Laboratory, Northwest Institute of Nuclear Technology, Xi'an, P.R. China
3 Key Laboratory of Biomedical Information Engineering of Ministry of Education, School of Life Science and Technology, Xi'an Jiaotong University, Xi'an, P.R. China

* Dongsheng Kong, Wenyu Peng and Rui Zong contributed equally

Corresponding Author: Xinguang Yu, e-mail: xinguang_yu301@163.com

Source of support: This work was supported by the Science and Technology Commission of the Central Military Commission [grant numbers 17-163-12-ZT-006-003-03]

Background: With infiltration, high-grade glioma easily causes the boundary between tumor tissue and adjacent tissue to become unclear and results in tumor recurrence at or near the resection margin according to the incomplete surgical resection. Fourier transform infrared spectroscopy (FTIR) technique has been demonstrated to be a useful tool that yields a molecular fingerprint and provides rapid, nondestructive, high-throughput and clinically relevant diagnostic information.

Material/Methods: FTIR was used to investigate the morphological and biochemical properties of human astrocytes (HA), microglia (HM1900), glioma cells (U87), and glioblastoma cells (BT325) cultured *in vitro* to simulate the infiltration area, with the use of multi-peak fitting and principal component analysis (PCA) of amide I of FTIR spectra and the use of hierarchical cluster analysis (HCA).

Results: We found that the secondary structures of the 4 types of cells were significantly different. The contents of α -helix structure in glial cells was significantly higher than in the glioma cells, but the levels of β -sheet, β -turn, and random coil structures were lower. The 4 types of cells could be clearly separated with 85% for PC1 and 12.2% for PC2.

Conclusions: FTIR can be used to distinguish between human astrocytes, microglia, glioma, and glioblastoma cells *in vitro*. The protein secondary structure can be used as an indicator to distinguish tumor cells from glial cells. Further tissue-based and *in vivo* studies are needed to determine whether FTIR can identify cerebral glioma.

MeSH Keywords: **Astrocytes • Glioma • Microglia • Spectroscopy, Fourier Transform Infrared**

Abbreviations: **FTIR** – Fourier Transform Infrared; **PCA** – principal component analysis; **HCA** – hierarchical cluster analysis; **ATR** – attenuated total reflection; **ATCC** – American Type Culture Collection; **STR** – short tandem repeat; **DMEM** – Dulbecco's modified Eagle's medium; **EDTA** – Ethylene Diamine Tetraacetic Acid; **PBS** – phosphate-buffered saline; **BaF₂** – Barium fluoride; **RMieS** – resonant Mie scattering; **FBS** – fetal bovine serum

Full-text PDF: <https://www.medscimonit.com/abstract/index/idArt/925754>

 2768

 1

 6

 26



Background

Glioma is the most common primary brain tumor worldwide [1], and approximately 100 000 new cases are diagnosed every year [2]. Generally, surgical resection is the treatment of choice for glioma [3]. Although surgical resection can reduce the risk of malignancy [4], in high-grade gliomas tumor cells sometimes infiltrate into normal tissues by 4–7 cm and blur the boundaries between tumor tissues and normal tissues [5]. Moreover, this extent of tumor margin diffusion and infiltration cannot be fully characterized by conventional medical imaging [6], resulting in tumor recurrence at or near the resection margin due to incomplete surgical resection [7]. Therefore, for the surgical treatment of gliomas, it is essential to characterize the tumor as accurately as possible to achieve an accurate and timely diagnosis of brain glioma and establish a targeted treatment plan.

FTIR spectroscopy has been demonstrated to be an effective and non-invasive diagnostic method that characterizes the biochemical changes in tissues, cells, and even at the molecular level [8]. Oligodendroglial and astrocytic tumor cells can easily be identified by their infrared spectra, with characteristic features in the lipid acyl chain region as well as in the nucleic acid region [9, 10]. For glioblastoma stem cells, attenuated total reflection (ATR) FTIR spectroscopy allows correct classification of the tissues, differentiating between CD133-rich and CD133-poor populations [11,12]. The main spectral differences were found in the 1000 cm^{-1} to 1150 cm^{-1} region, which can be assigned to vibrations of the chemical bonds in DNA, RNA, carbohydrates, and phospholipids. Extravascular diffusion of IR-absorbing nanoparticles can be imaged on histological slices by FTIR imaging, thus revealing morphological abnormalities in blood capillaries induced by angiogenetic stress [13]. Lei Li et al. applied FTIR spectra to the normal and several heterogeneous ovarian cancer cell lines and compared them in the spectral region of 4000–600 cm^{-1} , showing that protein conformation and composition are altered in some cancer cells [14]. Jitto Titus et al. used total reflectance Fourier transform infrared spectroscopy to show that after anti-TNF α therapy of colitis, the alpha helix/beta-sheet ratio recovered to the basal level [15].

This study aimed to use Fourier transform infrared spectroscopy (FTIR) to investigate the morphological and biochemical properties of human astrocytes, microglia, glioma, and glioblastoma cells cultured *in vitro*. These results will be useful in further research using FTIR imaging of the glioma infiltration area.

Material and Methods

Cell culture and sample preparation

Human astrocytes (HAs), human microglia (HM-1900), human glioma cells (U-87), and human brain pleomorphic glioblastoma cells (BT-325) were studied. All cells were purchased from the American Type Culture Collection (ATCC), (Manassas, VA, USA), and mycoplasma was routinely detected. At the same time, short tandem repeat (STR) tests were performed on the 4 cell types, and the test results indicated that no cross-contamination occurred. The cells were placed in Dulbecco's modified Eagle's medium (DMEM, Bio. Ind., Kibbutz Beit-Haemek, Israel) containing 10% fetal bovine serum (FBS, Gibco, Thermo Fisher Scientific, Waltham, MA, USA) and placed in a 37°C, 5% CO₂ incubator. When the cell growth density reached 90%, the cells were removed from the incubator and passaged at a ratio of 1: 3. During the third passage, preheated 0.25% trypsin containing ethylene diamine tetraacetic acid (EDTA, QIYI, Foshan, China) was used to digest cells in logarithmic growth phase, and then the cells were centrifuged at 1200 rpm for 5 min, and the supernatant was discarded. The cultured cells were rinsed twice with phosphate-buffered saline (PBS) solution, fixed in formalin for 30 min, rinsed with deionized water 3 times, centrifuged and concentrated to approximately 5×10⁸ cells/ml. Barium fluoride (BaF₂) slides were used as the substrate for spectrum collection; 40 μl of cell suspension was dropped onto the BaF₂ slides, then the slides placed in a drying oven ready for IR spectrum collection. All slides were photographed using an Olympus BX51 microscope. The cells were observed under the microscope when the concentration was about 80%. Six independent experiments were performed for each type of cell.

Infrared spectroscopic imaging

The absorbance spectra were collected using an FTIR Vertex 70v spectrometer (Bruker, Ettingen, Germany) at the National Defense Science and Technology Innovation Institute in Beijing. The range of the wavenumber was set as 4000–800 cm^{-1} with the resolution of 4 cm^{-1} and a spectrum was taken for 64 scans to improve the signal-to-noise ratio. To attenuate spectral distortion caused by Mie scattering (RMies), all the raw FTIR spectra were pre-processed with the RMies-EMSC algorithm. Because the band of amide II is largely not dependent on protein secondary structure, the corrected spectrum was normalized for equal absorption peak intensity in the position of amide II. All the data were collected by OPUS (Bruker, Ettingen, Germany) and pre-processed by MATLAB R2016b software (MathWorks, Natick, Massachusetts, USA).

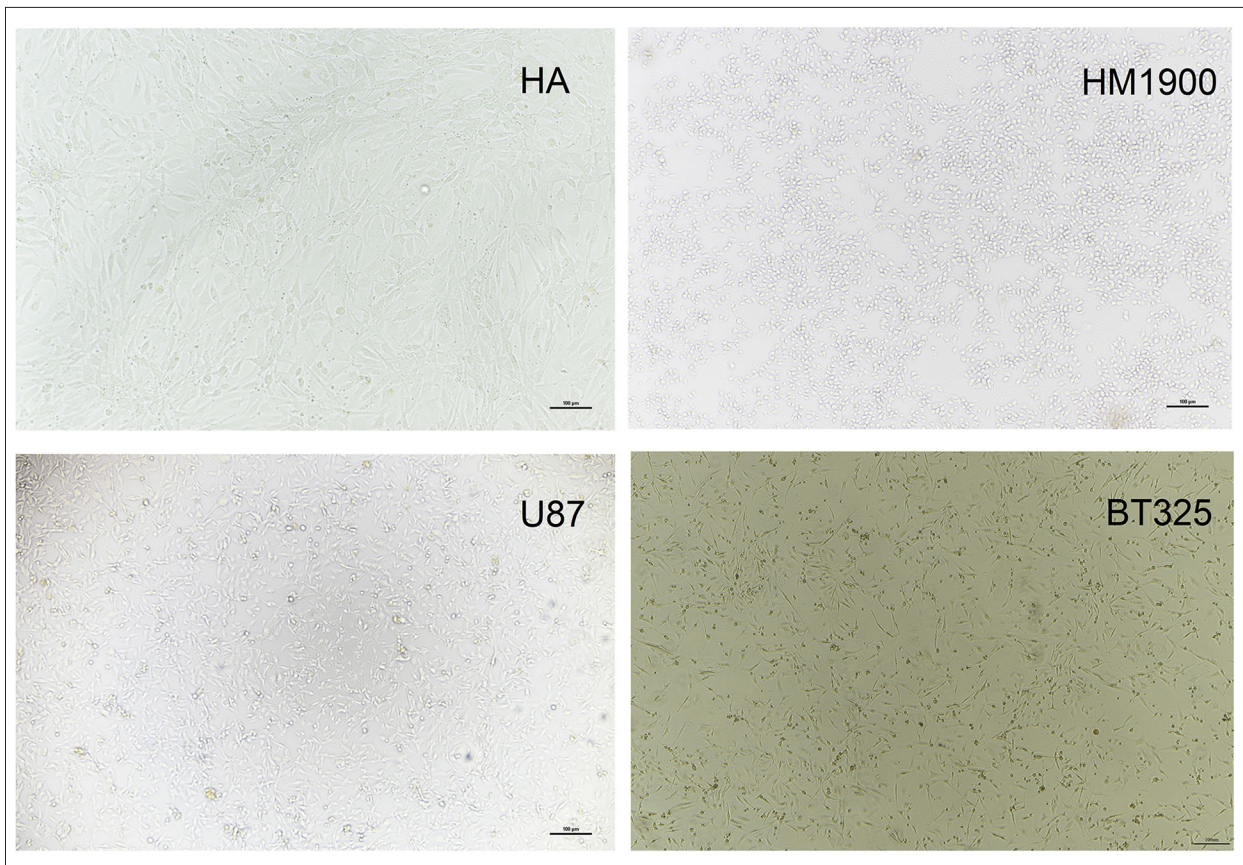


Figure 1. Cellular morphology of HA and HM-1900, U-87, and BT-325 cells *in vitro* (magnification 200×).

Data analysis

The analysis of difference of the spectrum was mainly based on the amide I band with the range of wavenumber 1600–1700 cm^{-1} , contributed to the C=O stretch containing protein-rich secondary structure information, such as α -helix, β -sheet, β -turn, random, and other undefined structures. Multi-peak curve fitting over this range was based on the second derivative of the spectrum, and the area percentage of each secondary structure was calculated. Meanwhile, the PCA and HCA were applied to the secondary derivative spectra of amide I, and the contribution of each secondary structure to the classification of the human neuroglial cells and glioma cells was analyzed through the loadings of PC1 and PC2.

Results

Cellular morphology of HAs and HM-1900, U-87, and BT-325 cells *in vitro*

The morphological characterization of cells is very important for showing the physiological state. An inverted microscope was used to examine the cell morphology (Figure 1). HA cells

have an elongated axis with an oval or circular nucleus in the center. HM1900 cells show round, small, and short rod-shaped with clear edges. The U87 cells show long fusiform or irregular shape with clear antennae, transparent cell body, and good refractive property. BT325 adherent cells are relatively small, showing a variety of shapes, including fusiform and star-shaped.

Mean FTIR spectra and second derivative spectra

Figure 2A shows all of the spectra of the 4 types of cells in the range of 1000–1800 cm^{-1} after Mie scattering correction and normalization of the amide II band peak. Figure 2A shows that the spectra of the different types of cells are similar to each other, including the positions and shapes of the absorption peaks, except for the amide I band (marked with the yellow region). Then, the second derivative of this range was calculated to better reflect the hidden peaks in the amide I band (Figure 2B). The results show that the second derivative of the glioma cells of U87 and BT325 has a similar shape, and has a significant difference from HA and HM1900. Although HA and HM1900 belong to the glial cell lines, there are still obvious differences between the 2 types of cells. This phenomenon is explained in detail by the results of the multi-peak fitting, which represents the protein secondary structure components.

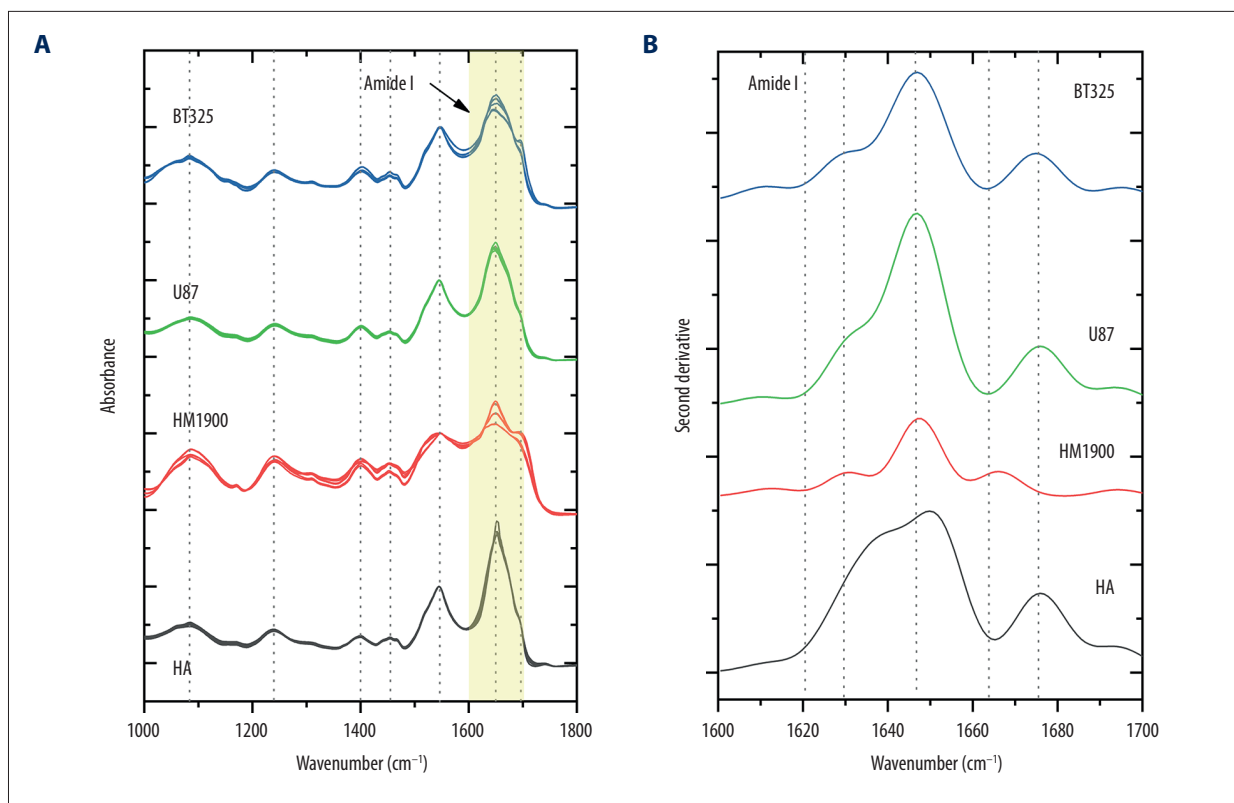


Figure 2. FTIR spectra in the range of 1000–1800 cm⁻¹ (A) and the corresponding second derivative spectra of HA, HM1900, U87 and BT325 cells in amide I band (B).

Secondary structure components

According to the second derivative spectrum, the secondary structure components of the 4 types of cells in the range of amide I band are shown in Figure 3. Generally, the band at 1653±4 cm⁻¹ is attributed to the α -helix structure, β -sheet structure often appears at 1620 cm⁻¹ and 1640 cm⁻¹, β -turn structure occurs at around 1665 cm⁻¹, 1670 cm⁻¹, 1675 cm⁻¹, 1683 cm⁻¹, 1688 cm⁻¹, and 1694 cm⁻¹, and the random structures are usually found at 1637 cm⁻¹ and 1648 cm⁻¹. For the second derivative spectrum of HA, there are 6 absorption peaks in the range of 1600–1700 cm⁻¹: 1612 cm⁻¹, 1629 cm⁻¹, 1639 cm⁻¹, 1651 cm⁻¹, 1675 cm⁻¹, and 1694 cm⁻¹ (Figure 3A). The peaks of 1629 cm⁻¹, 1633 cm⁻¹, and 1637 cm⁻¹ are attributed to β -sheet structure, 1651 cm⁻¹ is attributed to α -helix structure, and the positions of 1675 cm⁻¹ and 1694 cm⁻¹ are attributed to β -turn structure. For the secondary structure of HM1900 (Figure 3B), there are 7 absorption peaks in the range of amide I: 1608 cm⁻¹, 1614 cm⁻¹, 1630 cm⁻¹, 1645 cm⁻¹, 1648 cm⁻¹, 1666 cm⁻¹, and 1694 cm⁻¹. There is only 1 β -sheet structure sub-band appearing in 1630 cm⁻¹; 1645 cm⁻¹ belong to the random coil structure, the sub-band of 1648 cm⁻¹ is in the range of α -helix structure, and 2 β -turn structure sub-bands appeared in 1666 cm⁻¹ and 1694 cm⁻¹. For the human glioma cells of U87 and BT325, the protein secondary structures are

similar to each other, including the positions and numbers of the sub-band in the range of α -helix, β -sheet, β -turn, and random coil structure (Figure 3C, 3D).

Area percentage of α -helix, β -sheet, β -turn, and random coil structure

According to the results of the multi-peak curve fitting of the amide I, the area percentage of α -helix, β -sheet, β -turn and random coil structure of the Human glial cells and glioma cells were calculated and the result showed in Figure 4. From the Figure 4A, we can see that the contents of α -helix structure in human glial cells (HA, HM1900) were significantly higher than glioma cells, and according to the Student's t-test analysis, the P value were less than 0.01. However, for the β -sheet structure and random structure in the glioma cells of U87, the level has elevated relative to the HA and HM1900 cells and the difference is significant (P<0.01 and P<0.05, respectively). In addition, the BT325 cells show the highest content of β -turn structure among the 4 types of the cells and was significantly different from HM1900 (P<0.05). The secondary structure of amide I between the human glial cells of HA and HM1900, and between the human glioma cells of U87 and BT325, has no significant difference, which demonstrates that the when the glial cells become cancerous, the secondary structure of

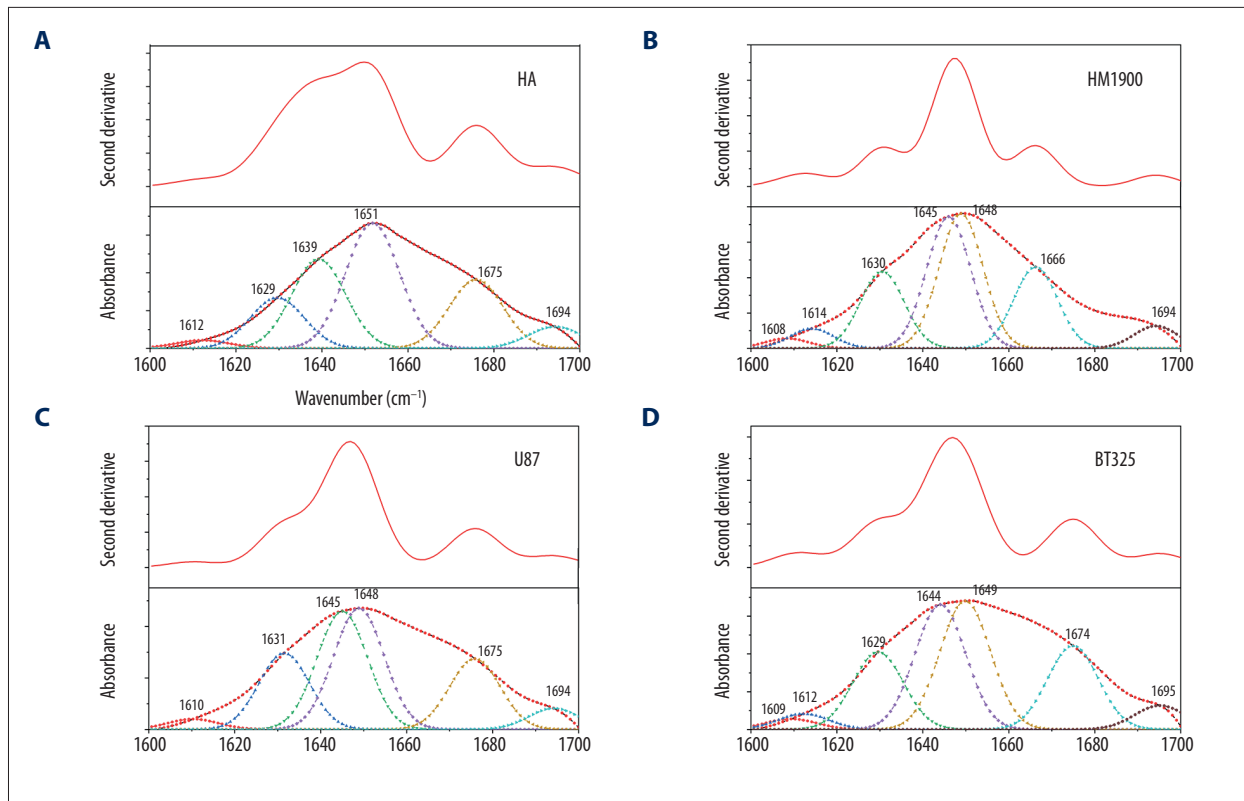


Figure 3. (A–D) Second derivative of amide I of the 4 types of cells and multi-peak curve fitting to obtain the protein secondary structure components according to the second derivative.

the protein also changes, which was manifested in less content of α -helical structure, and increased content of β -sheet, β -turn, and random structure.

PCA and HCA

PCA and HCA were applied to the second derivative spectra of the amide I band, and the results are shown in Figures 5 and 6. Figure 5A illustrates that the clusters of the spectra from the 4 types of cells were separated in the PC1 versus PC2 plane (elliptical line represents 95% confidence interval) and the first 2 PCs explained 97.2% of the total variance with 85.0% for PC1 and 12.2% for PC2. Figure 5B explained the clustering of the PCs scores, in which the PC1 score at 1652 cm^{-1} indicated a high level of α -helix secondary structures, which contributed most to the first principal component, and the band at 1675 cm^{-1} , which owned to β -turn, had a high level in PC2 loading. These results suggest that the content of the α -helix secondary structure may serve as an indicator to distinguish gliomas from glial cells.

HCA results (Figure 6) show that the distance between U87 and BT325 was the closest among the 4 types of cell, which illustrated similar spectral information between the 2 kinds of cells, followed by HA, but the distance was farthest for HM1900,

which means a relatively large difference in spectral information vs. glioma cells.

Discussion

Glioma refers to all tumors of glioma origin, including astrocytoma, oligodendroglioma, ependymoma, and mixed glioma. Astrocytoma includes astrocytoma (grades I and II), anaplastic astrocytoma (grade III), and glioblastoma (grade IV) [16,17]. When affected by gliomas, the brain undergoes reactive gliosis, vascular proliferation, and inflammatory cell infiltration. Reactive astrocytosis is a common feature of gliomas and is usually confined to the immediate vicinity of the tumor [18]. Microglial cells and macrophages, as the main infiltrating immune cell population, account for 13–34% and 4.2–12% of the tumor cell volume in experimental gliomas, respectively [19], and participate in creating a microenvironment conducive to the growth of gliomas [20,21]. The whole range of the infrared spectrum can be divided into 2 regions of functional groups (4000–1300 cm^{-1}) and fingerprint regions (1300–600 cm^{-1}). Peaks in the functional group region are absorption bands generated by stretching vibrations. In the fingerprint region, in addition to stretching vibrations of a single bond, there is a complex spectrum due to deformation vibrations [22]. According

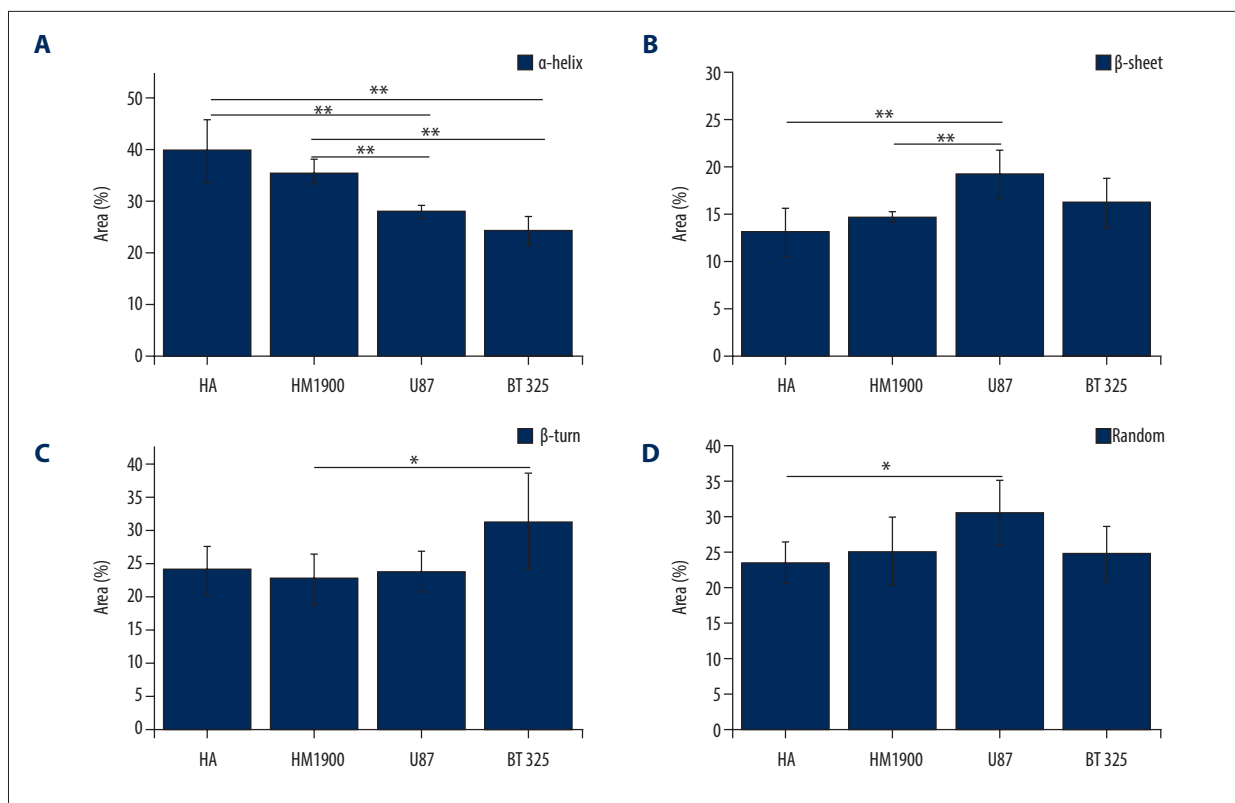


Figure 4. Percentage of secondary structures of protein Amide I in glial cells and glioma cells. (A) α-helix structure, (B) β-sheet structure, (C) β-turn structure, (D) random structure. Error bars represent the SEM, n=6 (* $P<0.05$; ** $P<0.01$).

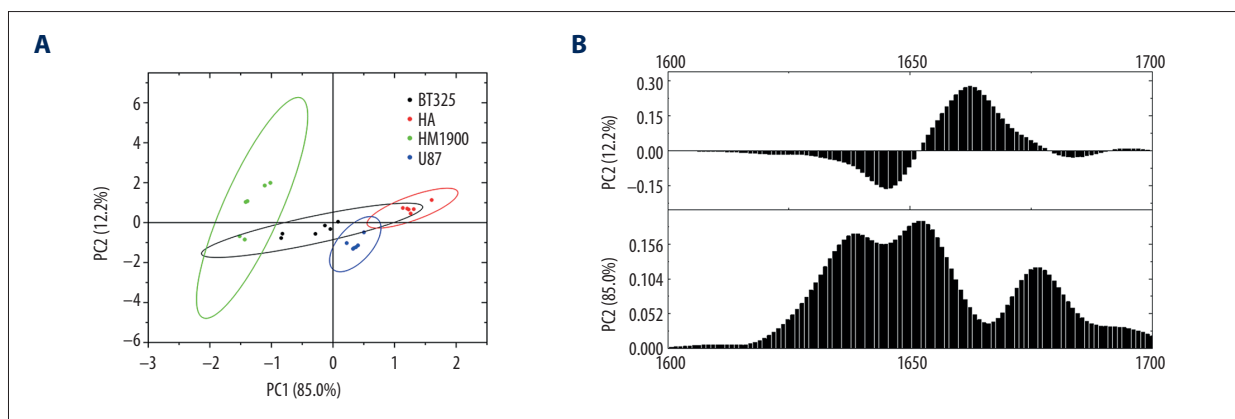


Figure 5. (A, B) PCA analysis applied to the range of amide I and the loadings of PC1 and PC2.

to different biological components, the spectrum can be divided into fatty acid (3000–2800 cm^{-1} , acyl chain stretching vibrations, with the fatty acids of lipids as main contributors; 1480–1300 cm^{-1} , deformation vibrations of CH₂ and CH₃ alkyl groups), protein (1800–1480 cm^{-1} , amide I and II bands that arise from C=O stretching and N–H bending vibrations) and nucleic acid and sugar (1300–900 cm^{-1} , symmetric and antisymmetric stretching vibrations of phosphodi-oxo groups, PO₂) regions [23,24]. The assignments of the main bands are given in Table 1.

In this study, we applied a label-free spectroscopy technique of FTIR to the glial and glioma cell lines, which were HA, HM1900, U87, and BT325 cells. Through multi-peak fitting according to the second derivative of amide I band, we found that the contents of the protein secondary structure in the glial cell lines and glioma cells were significantly different, indicating that the level of the secondary structure had changed in the canceration process of glioma cells, which was manifested in lower content of α-helical structure, and increased content of β-sheet, β-turn, and random structure.

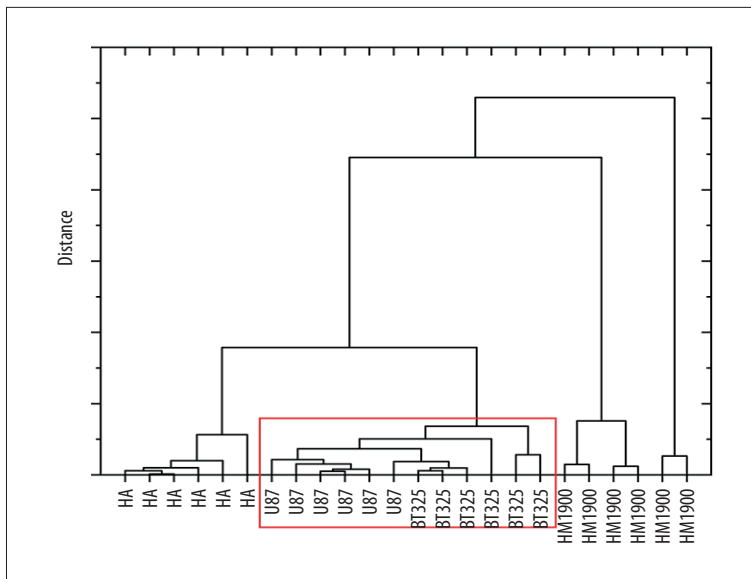


Figure 6. HCA analysis applied to the range of amide I.

Table 1. Assignment of the most prominent absorption bands.

Peak ID	Band/cm ⁻¹	Assignment
1	965–980	C-C, PO ₄ -stretch: DNA, RNA, phospholipids
2	1039	C-O-H deformation: glycogen
3	1070–1150	C-O-C and C-C stretch: carbohydrates, lipids, glycolipids
4	1083–1085	PO ₂ -symmetric stretch: nucleic acids in DNA and RNA
5	1172	C-O (H) stretch: carbohydrates
6	1237–1244	PO ₂ -asymmetric stretch: nucleic acids, lipids
7	1277	C-H/N-H deformation: amide III, components of proteins
8	1393–1402	-COO-symmetric stretch: fatty acids, amino acids
9	1450–1454	CH ₂ , CH ₃ deformation: mainly lipids, proteins
10	1538–1546	N-H bend (60%), C-N stretch (40%) and C-C stretch: amide II, peptide, proteins (α-helix, β-sheets, turn and random coil)
11	1600–1706	C=O stretch (76%), C-N stretch (14%), CNN (10%): amide I, proteins (α-helix, β-sheets, turn and random coil)
12	1746	C=O stretch: esters (lipids, phospholipids)
13	1700–1799	C=O deformation: lipids
14	2844–2860	-CH ₂ symmetric stretch: lipids
15	2892–2924	-CH ₃ symmetric stretch: lipids
16	2953–2994	-CH ₃ asymmetric stretch: lipids
17	3099–3296	-NH ₂ symmetric stretch: amide B, peptides, proteins
18	3327–3337	-NH ₂ asymmetric stretch: amide A, peptides, proteins

Protein secondary structure provides significant insight into structural features and is critical to biological function, which is determined by the set of dihedral angles (ϕ , ψ) and defines the spatial orientation of the peptide backbone and the presence of specific hydrogen bonds [25]. Generally, α -helix conformation has strong amide I bands in the range of 1650 cm^{-1} and 1655 cm^{-1} and β -sheet structure usually has strong bands between 1612 cm^{-1} and 1640 cm^{-1} and some low frequencies of $1665\text{--}1670\text{ cm}^{-1}$. The unordered or random structure is generally assigned to the band near 1645 cm^{-1} . Multi-peak curve fitting of amide I IR band according to the second derivative gives a reasonably accurate estimate of the content of the protein secondary structure. The results illustrated that the content of α -helix structure in glial cells was significantly higher than that in the glioma cells, and the content of the β -sheet, β -turn, and random structure were relatively lower; these changes may be closely related to the cell function.

Glioma is a complex ecosystem composed of various cellular components and non-cellular components, including microglia, stem cells, astrocytes, endothelial cells, and glioma cells, and the non-cellular components of extra-cellular matrix (ECM), cytokines, and growth factors. The types of cells studied in this article obviously cannot simulate the real internal environment of glioma tissues, but this research illustrated that the content of protein secondary structure in different cell types is different and FTIR spectroscopy could be used to characterize this change. Razia Noreen et al. reviewed the FTIR image of collagen in the process of glioma development and concluded that FTIR spectroscopy can distinguish several types of collagen based on their secondary structure content, and the spectral

data from FTIR images can be mathematically re-constructed according to the secondary structure parameters [26], which suggests that the glioma infiltration area of FTIR image could be re-constructed according to the content of the protein secondary structure, and the edge information could be displayed and may guide clinical surgery in the future.

However, there were also some limitation to our study. This study did not detect live cells, and live cell detection is closer to the physiological state. Purified glioma cell lines are different from glioma cells under pathological conditions, and reactive glioma cells may have different cellular components. Although glioma tissue is rich in tumor cells, cell detection is different from tissue detection. There is still a long way to go before using FTIR to differentiate glioma tissue from normal brain tissue.

Conclusions

In this study, we evaluated the potential of label-free vibrational spectroscopic techniques to detect sample biochemical components to identify microglia, astrocytes, and glioma cells. The difference in the relative contents of lipids, glycogen, proteins, and other components was used to distinguish astrocytes, microglial cells, and 2 different glioma cell lines. These differences in cell components further differentiated the boundaries of gliomas to supplement and support previous data. These results may also be used to find new targets for further understanding glioma metabolism and new strategies for glioma treatment, which has broad application prospects.

References:

- Ostrom Q, Gittleman H, Stetson L et al: Epidemiology of gliomas. *Cancer Treat Res*, 2015; 163: 1–14
- Bray F, Ferlay J, Soerjomataram I et al: Global cancer statistics 2018: GLOBOCAN estimates of incidence and mortality worldwide for 36 cancers in 185 countries. *CA Cancer J Clin*, 2018; 68(6): 394–424 [Erratum in: *Cancer J Clin*, 2020; 70(4): 313]
- Bush NA, Chang SM, Berger MS: Current and future strategies for treatment of glioma. *Neurosurg Rev*, 2017; 40(1): 1–14
- Bahreini M: Role of optical spectroscopic methods in neuro-oncological sciences. *J Lasers Med Sci*, 2015; 6(2): 51–61
- Ferrer VP, Moura Neto V, Mentlein R: Glioma infiltration and extracellular matrix: key players and modulators. *Glia*, 2018; 66(8): 1542–65
- Chang PD, Chow DS, Yang PH et al: Predicting glioblastoma recurrence by early changes in the apparent diffusion coefficient value and signal intensity on FLAIR images. *Am J Roentgenol*, 2017; 208(1): 57–65
- Zhang J, Liu H, Tong H et al: Clinical applications of contrast-enhanced perfusion MRI techniques in gliomas: Recent advances and current challenges. *Contrast Media Mol Imaging*, 2017; 2017: 7064120
- Hu R, Zong C, Lin L-x et al: Chemical analysis of live cell activities by Fourier transform infrared (FTIR) spectroscopy in transmission mode. *Vibrational Spectroscopy*, 2020; 103068
- Sabbatini S, Conti C, Orilisi G, Giorgini E: Infrared spectroscopy as a new tool for studying single living cells: Is there a niche? *JBS Imaging*, 2017; 6(3–4): 85–99
- Singh B, Boopathy S, Somasundaram K, Umapathy S: Fourier transform infrared microspectroscopy identifies protein propionylation in histone deacetylase inhibitor treated glioma cells. *J Biophotonics*, 2012; 5(3): 230–39
- Uckermann O, Juratli TA, Galli R et al: Optical analysis of glioma: Fourier-transform infrared spectroscopy reveals the IDH1 mutation status. *Clin Cancer Res*, 2018; 24(11): 2530–38
- Rabe J-H, Sannour DA, Schulz S et al: Fourier transform infrared microscopy enables guidance of automated mass spectrometry imaging to pre-defined tissue morphologies. *Sci Rep*, 2018; 8(1): 1–11
- Talari ACS, Martinez MAG, Movasaghi Z et al: Advances in Fourier transform infrared (FTIR) spectroscopy of biological tissues. *JASR*, 2017; 52(5): 456–506
- Li L, Bi X, Sun H et al: Characterization of ovarian cancer cells and tissues by Fourier transform infrared spectroscopy. *J Ovarian Res*, 2018; 11(1): 64
- Titus J, Ghimire H, Viennois E et al: Protein secondary structure analysis of dried blood serum using infrared spectroscopy to identify markers for colitis screening. *J Biophotonics*, 2018; 11(3): e201700057
- Hanif F, Muzaffar K, Perveen K et al: Glioblastoma multiforme: A review of its epidemiology and pathogenesis through clinical presentation and treatment. *Asian Pac J Cancer Prev*, 2017; 18(1): 3–9
- Tamimi AF, Juweid M: Epidemiology and outcome of glioblastoma. In: *Glioblastoma*. Codon Publications, 2017
- Bárdos H, Molnár P, Csecsei G, Ádány R: Composition of the extracellular matrix in human gliomas. In: *Tumor matrix biology*. CRC Press, 2017; 131–44

19. Gutmann DH, Kettenmann H: Microglia/brain macrophages as central drivers of brain tumor pathobiology. *Neuron*, 2019; 104(3): 442–49
20. Hambardzumyan D, Gutmann DH, Kettenmann H: The role of microglia and macrophages in glioma maintenance and progression. *Nat Neurosci*, 2016; 19(1): 20–27
21. Wei J, Chen P, Gupta P et al: Immune biology of glioma-associated macrophages and microglia: Functional and therapeutic implications. *Neuro Oncol*, 2020; 22(2): 180–94
22. Wiercigroch E, Szafraniec E, Czamara K et al: Raman and infrared spectroscopy of carbohydrates: A review. *Spectrochim Acta A Mol Biomol Spectrosc*, 2017; 185: 317–35
23. Thompson JM. *Infrared spectroscopy*. CRC Press, 2018
24. Fleming I, Williams D: Infrared and raman spectra. In: *Spectroscopic methods in organic chemistry*. Springer, 2019; 85–121
25. Pelton JT, McLean LR: Spectroscopic methods for analysis of protein secondary structure. *Anal Biochem*, 2000; 277(2): 167–76
26. Noreen R, Moenner M, Hwu Y, Petibois C: FTIR spectro-imaging of collagens for characterization and grading of gliomas. *Biotechnol Adv*, 2012; 30(6): 1432–46